European Journal of Chemistry 16 (1) (2025) 7-19

EurjChem An International Open Access Journal European Journal of Chemistry ATLANTA PUBLISHING HOUSE

The role of water and iodine in supramolecular assembly of a 2D coordination of benzimidazole derivate: X-ray crystallography and DFT calculations

Sahajkumar Anilkumar Gandhi [1,*], Saurabh Soni [2], Urmila Patel [3] and Deepali Kotadia [2]

[1] *Department of Physics, Bhartiya Vidya Bhavan's Shri Ishvarlal Laxmiprasad Pandya Arts-Science and Jashodaben Shah Commerce College, Dakor-388225, Gujarat, India*
[2] *Department of Chemistry, Sardar Patel University, Vallabh Vidyanagar-388120, Gujarat, India*
[3] *Department of Physics, Sardar Patel University, Vallabh Vidyanagar-388120, Gujarat, India*

* *Corresponding author at: Department of Physics, Bhartiya Vidya Bhavan's Shri Ishvarlal Laxmiprasad Pandya Arts-Science and Jashodaben Shah Commerce College, Dakor-388225, Gujarat, India.*
e-mail: sahajg7@gmail.com (S.A. Gandhi).

RESEARCH ARTICLE

10.5155/eurjchem.16.1.7-19.2602

Received: 08 October 2024
Received in revised form: 16 December 2024
Accepted: 14 January 2025
Published online: 31 March 2025
Printed: 31 March 2025

KEYWORDS

DFT calculation
Single crystal structure
Molecular docking study
Hirshfeld surface analysis
Benzimidazole derivatives
Hydrogen bond interactions

ABSTRACT

To understand the relationships between molecular structure and properties, as well as to validate predictive models, density functional theory (DFT) and experimental characterization of molecules are essential. In this study, we describe the synthesis and crystal structure of the 1,3-dimethyl-3*H*-benzimidazol-1-ium iodide monohydrate (DBZIW), which crystallizes in a monoclinic system with the space group $P2_1/c$, a = 8.9323(4) Å, b = 7.1654(3) Å, c = 17.6425(8) Å, β = 101.432(2)°, V = 1106.78(8) Å^3, Z = 4, T = 293(2) K, μ(MoKα) = 2.860 mm^{-1}, $Dcalc$ = 1.753 g/cm^3, 9452 reflections measured (4.652° ≤ 2Θ ≤ 55.512°), 2547 unique (R_{int} = 0.0244, R_{sigma} = 0.0222) which were used in all calculations. The asymmetric unit comprises a $[C_9H_{11}N_2]^+$ molecule, an iodine ion (I^-), and a water molecule. The B3LYP/6-311++G(d,p) diffuse function was used to optimize the structures of 1,3-dimethyl-3*H*-benzimidazol-1-ium (DBZ) and 1,3-dimethyl-3*H*-benzimidazol-1-ium monohydrate (DBZW), while the structures of 1,3-dimethyl-3*H*-benzimidazol-1-ium iodine (DBZI) and 1,3-dimethyl-3*H*-benzimidazol-1-ium iodide monohydrate (DBZIW) were optimized using the B3LYP/Def2-TZVP method due to the presence of the iodine ion. These optimizations were performed using Gaussian09 software, and both models accurately predicted the bond lengths, bond angles, and torsion angles of the molecules. Furthermore, DFT calculations were employed to determine the HOMO-LUMO energy levels, energy gap, softness, hardness, and other quantum chemical parameters. A strong intermolecular hydrogen bond interaction, along with the aromatic ring system and the fusion of benzene and imidazole, constitutes a small but highly significant structure that has been confirmed. The O1 atom of the water molecule and the iodine ion (I^-) participate in a significant hydrogen bond interaction (O-H···I) within the molecular packing of DBZIW. Furthermore, the network of C-H···O hydrogen bond contacts plays a crucial role in the stability of the structure. Hirshfeld surface analysis was carried out to identify the various hydrogen bonds. The energy frameworks for the compounds were constructed through based on intermolecular interaction energies to know ascertain dominant interaction energy involved contributing to the strength of the packing. Molecular studies indicated that DBZIW had exhibits high binding affinity for thyroid-stimulating hormone receptor (TSHR) protein targets (4QT5).

Cite this: *Eur. J. Chem.* **2025**, *16(1)*, 7-19 **Journal website**: www.eurjchem.com

1. Introduction

Benzimidazole is characterized by a notable heterocyclic structure that is frequently observed in biological systems, as well as in the naturally occurring compound cyanocobalamin. Its distinctive structural properties and electron-rich environment make benzimidazole a valuable component in the pharmaceutical sector for drug development. The diverse pharmacological attributes of benzimidazole derivatives, which encompass antibacterial, antiviral, antioxidant, and anticancer effects, highlight their importance in the field of medical research [1-10]. Beyond their biological applications, benzimidazole derivatives have garnered significant interest in the field of materials science. This is attributed to their ability to crystallize into materials that exhibit exceptional conductivity and ferroelectric properties, which arise from intramolecular and intermolecular hydrogen bonding interactions [11-14]. Additionally, these derivatives have environmental implications when utilized as preservatives in the manufacturing processes of paints, textiles, and paper, as well as in the formulation of biopesticides aimed at addressing plant diseases. Furthermore, research conducted by Walid Ettahiri *et al.* has shown that these compounds possess anticorrosive properties and can function as corrosion inhibitors for mild steel [15-19].

ISSN 2153-2249 (Print) / ISSN 2153-2257 (Online)
https://dx.doi.org/10.5155/eurjchem.16.1.7-19.2602

Table 1. Crystal data and structure refinement parameters for the title compound.

Empirical formula	**$C_9H_{13}N_2IO$**
Formula weight (g/mol)	292.11
Temperature (K)	298(2)
Wavelength	MoKα (0.71073 Å)
Crystal system	Monoclinic
Space group	$P2_1/c$
Crystal size	$0.08 \times 0.04 \times 0.03$ mm^3
a, (Å)	8.9323(4)
b, (Å)	7.1654(3)
c, (Å)	17.6425(8)
β (°)	101.432(2)
Volume (Å^3)	1106.78(8)
Z	4
ρ_{calc} (g/cm^3)	1.753
F(000)	568
θ range for data collection	2.326 to 27.756°
Index ranges	$-11 \le h \le 11$; $-9 \le k \le 6$; $-21 \le l \le 22$
Reflections collected/unique [R(int)]	9452/ 2128 [0.024]
Completeness to θ max (%)	0.999
Refinement method	Full Matrix Least Square of $\|F\|^2$
Data/restrains/parameters	2128/7/ 128
Goodness-of-fit on F^2	1.077
Final R indexes [I≥2σ (I)]	R1 = 0.0311, wR2 = 0.0858
Final R indexes [all data]	R1 = 0.0387, wR2 = 0.0912
Largest diff. peak/hole (e.Å^{-3})	1.11 and -0.50
Software used to data collection	Bruker Kappa Apex-II
Software used to cell refinement	Bruker SAINT
Software used to solve the structure	SHELXS - 97
Software used to refine the structure	SHELXL - 2016

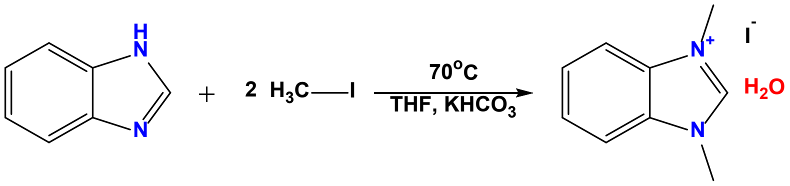

Scheme 1. The reaction scheme of the compound 1,3-dimethyl-3*H*-benzimidazol-1-ium iodide monohydrate.

Density functional theory (DFT) has emerged as a pivotal approach for exploring the relationship between the chemical and structural properties of small molecules [20,21]. In this context, and as part of our ongoing research [22-26] on X-ray crystallography and computational chemical analyses of synthesized compounds, we present the synthesis of a notable new derivative of benzimidazole, specifically 1,3-dimethyl-3*H*-benzimidazol-1-ium iodide monohydrate [DBZIW]. This study emphasizes the spectroscopic characterization of the compound through single crystal X-ray diffraction. We provide a comparative analysis of the X-ray diffraction data obtained from the single crystal (Experimental) alongside the theoretical results derived from quantum chemical calculations conducted using Gaussian software, which elucidate the electronic structure of the compound (Theoretical). To further investigate the electronic and structural properties of the molecules, we conducted calculations of the highest occupied molecular orbital (HOMO) and lowest unoccupied molecular orbital (LUMO), as well as Hirshfeld surface analysis employing three-dimensional energy frameworks.

2. Experimental

2.1. Materials and instrumentations

All reagents and solvents were purchased from Sigma-Aldrich and Alfa-Aesar. All solvents were distilled off and properly dried before use. The melting points were determined on an electrothermal melting point apparatus. The completion of the reaction and the purity of all compounds were verified on aluminum-coated TLC plates $60F_{245}$ (E. Merck) using *n*-hexane: ethyl acetate (7.5:2.5, v:v) as mobile phase and visualized under ultraviolet (UV) light, or iodine vapor. Elemental analysis (% C, H, N) was performed using a PerkinElmer 2400CHN analyzer. IR spectra were recorded on a PerkinElmer FT-IR spectrophotometer in KBr. The ^1H NMR and ^{13}C NMR spectra were recorded on a Varian Gemini 300 MHz and Varian Mercury-400 (100 MHz) instrument in $CDCl_3$ and MeOD as solvents and tetramethylsilane (TMS) as an internal standard. The mass spectrum was scanned on a Shimadzu LCMS 2010 spectrophotometer.

2.2. Synthesis of 1,3-dimethyl-3H-benzimidazol-1-ium iodide monohydrate (DBZIW)

THF (20 mL) was heated to 70 °C while methyl iodide (12.2 mmol) and 1*H*-benzimidazole (12 mmol) were added. After 24 hours, a small amount of THF. Dichloromethane (DCM) (30 mL) was used to dissolve the oil and $KHCO_3$ and around 3 mL of water were added. After the evolution of CO_2 stopped, the mixture was mixed again and a significant amount of $KHCO_3$ was added to absorb the water. The THF was separated from the reaction mass after the solution had been heated to 70 °C for 18 hours (Scheme 1). After being cleaned with ether and dried, the product was left in the form of tiny crystals. There were no impurities found during the synthesis of DWZIW. The melting point and recrystallization technique was used to confirm purity in addition to TLC analysis. Moreover, the ^1H and ^{13}C NMR technique is used to confirm the chemical structure. Here, we had used a slow evaporation method to grow single crystals. We used commonly methanol, ethanol, or acetone solvents to grow the single crystals. We got transparent needle shaped single crystals in ethanol solvents after a few months.

Table 2. Parameters used for docking in the HEX 8.0.0 program.

Parameter **Correlation type**	**Value** **Shape + Electro + DARS**	**Description**
Grid dimension	0.6	With 100 solutions
Receptor range	180	With step size 7.5
Ligand range	180	With step size 7.5
Twist range	360	With step size 5.5
Distance range	40	With box size 10
Scan step	0.8	-
Final scan	25	-

1,3-Dimethyl-3H-benzimidazol-1-ium iodide monohydrate (DBZIW): Color: White. Yield: 82%. M.p.: 192-196 °C. ^{1}H NMR (300 MHz, $CDCl_3$, δ, ppm): 9.35 (s, 1H, CH), 7.83-7.86 (t, 2H, CH), 7.61-7.65 (d, 2H, CH), 4.05 (s, 6H, CH_3). ^{13}C NMR (100 MHz, MeOD, δ, ppm): 142.6, 132.1, 126.7, 112.9, 32.8.

2.3. Crystallographic analysis

Three-dimensional X-ray crystallographic data of an optimum size single crystal (DBZIW) is collected at room temperature on a Bruker Kappa Apex-II diffractometer in the ω-2θ scan mode with graphite monochromatic MoKα radiation (λ = 0.71073 Å) at 298(2) K. Bruker SAINT software was used to obtain cell refinements and data reductions [27]. In order to characterize the thermal motion that causes the non-hydrogen atoms to fall, the structure was first solved using direct methods using SHELXS-97 [28] and then refined using full-matrix least squares based on F^2 with anisotropic thermal parameters using SHELXL-2016 [29]. Details of the data collection refinement parameters are in Table 1.

2.4. Computational details

The B3LYP method represents a hybrid approximation for the exchange-correlation functional, renowned for its ability to yield highly accurate results, which has led to its widespread application in computational chemistry. In this context, dispersion (van der Waals) interactions are critical to understanding the formation, stability, and functionality of molecules. However, it is important to note that popular local or semilocal exchange-correlation functionals lack the long-range correlation that is fundamental to dispersion interactions. Consequently, the incorporation of appropriate dispersion corrections is essential for density functional theory (DFT) calculations involving realistic molecular systems. In our study, we conducted quantum chemical computations utilizing an advanced theoretical framework to investigate the role of water and iodine. Geometrical optimization for DBZ, DBZW, DBZI, and DBZIW was performed using the B3LYP exchange correlation functional in conjunction with a 6-311++G(d,p) basis set, as well as def2-TZVP models for dispersion correction, while maintaining a minimal computational overhead relative to conventional DFT approaches [30-32]. The computations were executed using the Gaussian 09 software package, complemented by the Gauss-View molecular visualization tool [33,34].

2.5. Hirshfeld surface analyses

The software Crystal Explorer21 [35,36] offers a valuable feature to characterize the surface properties of molecules and serves as an effective tool to analyze intermolecular interactions within a crystal structure. This analysis provides insight into the intermolecular interactions present in the crystalline state, as it delineates the regions where molecules interact. The Hirshfeld surface, which envelops a molecule, is defined by the points at which the electron density contribution from the molecule of interest is equivalent to the electron density contributions from all other surrounding molecules. The distinctive capability of this method to compute and visually represent these interactions, yielding unique results for each crystal structure, underscores its significance. Analysis is carried out using the molecule's crystallographic information file (CIF). Among the primary functionalities of Hirshfeld surface analyses are the generation of two-dimensional fingerprint plots and three-dimensional molecular surface contours. These visualizations produce the van der Waals (vdW) surface surrounding the molecule, illustrating the spatial occupation of the molecule within the crystal structure. The contact distances between points on this surface and the atoms located inside (d_i) and outside (d_e) the surfaces are significantly influenced by the varying vdW radii of the constituent atoms, allowing for the normalization of these distances (d_{norm}). This methodology also facilitates a comprehensive examination of intermolecular interactions, ranging from short to long distances, within a crystal structure. The visualization of these interactions is conveyed through color-coded fingerprint plots and contour surfaces, where distances shorter than or longer than the sum of the vdW radii are represented in a spectrum from red (indicating shorter distances) to white and blue (indicating longer distances). Utilizing Crystal Explorer, the qualitative and quantitative data regarding the molecular interactions of the Benzimidazole derivative were investigated through a calculated energy framework.

2.6. Molecular docking study

Iodine is a commonly used antiseptic and is included in the World Health Organization (WHO) list of essential drugs, as it is a nutrient that the human body cannot synthesize independently [37]. It plays a vital role in human nutrition, particularly as a necessary element for the production of thyroid hormones. Insufficient iodine levels can impede the synthesis of these hormones, leading to potential health complications. A deficiency of iodine during pregnancy can cause conditions such as goiter, hypothyroidism, and cognitive impairment in both children and newborns. The thyroid stimulating hormone receptor (TSHR) was selected as the target molecule based on a review of existing literature [38,39] and empirical studies; its structural data were obtained from the Protein Data Bank (PDB) under the identifiers 2XW7, 4QT5 and 7XW7. The Hex software [40], an interactive tool for molecular docking studies, was used for this investigation. Hex is capable of processing PDB files for protein structures and SDF files for small molecules. The Hex 8.0.0 application, installed on a Windows operating system, facilitated the execution of blind-docking experiments. Three distinct methodologies were implemented in three separate experiments involving optimized protein structures, in which pharmaceuticals acted as ligands and protein served as the receptor: Shape (and only Shape), Shape + Electrostatic, and Shape + Electrostatic + DARS with macro sampling. These methodologies were employed to assess the structural compatibility of compounds with the active sites of proteins, as well as to evaluate nonbonding interactions, including electrostatic forces and hydrogen bonds. The optimal pose and binding energies for 100 different configurations were recorded. The docking parameters for the HEX 8.0.0 software are presented in Table 2.

Table 3. Bond distance (Å), bond angle (°), and torsion angles (°) involving non-hydrogen atoms by X-ray diffraction data (with estimated standard deviation in parentheses).

Bond lengths (Å)	X-ray	Bond Angles (°)	X-ray	Torsional Angles (°)	X-ray
N1- C1	1.330(4)	C1- N1- C5	108.1(3)	C9-C4-C5-C6	-0.7(5)
N1- C2	1.461(4)	C1- N1- C2	125.8(3)	C9-C4-C5-N1	179.4(3)
N1- C5	1.392(4)	C5- N1- C2	126.1(3)	N1-C5-C6-C7	-179.8(3)
N2- C1	1.331(4)	C1- N2- C4	108.0(3)	C3-N2-C4-C9	1.8(6)
N2- C3	1.463(4)	C1- N2- C3	126.3(3)	C3-N2-C1-N1	178.6(3)
N2- C4	1.392(4)	C4- N2- C3	125.7(3)	C2-N1-C1-N2	179.5(3)
C4- C5	1.378(5)	N1- C1- N2	110.2(3)		
C4- C9	1.396(5)	C5- C4- N2	106.9(3)		
C5- C6	1.386(5)	C5- C4- C9	121.9(3)		
C6 -C7	1.364(6)	N2- C4- C9	131.1(3)		
C7 -C8	1.412(7)	C4- C5- C6	122.2(3)		
C8 -C9	1.371(6)	C4- C5- N1	106.7(3)		
		C6- C5- N1	131.2(3)		
		C7- C6- C5	116.3(4)		
		C6- C7- C8	121.9(4)		
		C9-C8- C7	121.7(4)		
		C8-C9- C4	115.9(4)		
		H11-OW1- H12	117.0(2)		

Table 4. Hydrogen bond and π-π interactions of the title molecule *.

D-H···A	D-H, Å	D-A, Å	H···A, Å	∠D-H···A, °	
C2-H2A···OW1 (i)	0.960(4)	3.519(7)	2.660(6)	149.19(29)	
C6-H6···OW1 (i)	0.930(4)	3.620(8)	2.786(6)	149.68(28)	
OW1-H1B···I (ii)	0.859(5)	3.647(4)	2.883(4)	158.69(20)	
Cg(I)-Cg(J)	**Cg(I)···Cg(J), Å**	**α, °**	**β, °**	**γ, °**	**Cg(I)···P, Å**
Cg(1)-Cg(2) (iii)	3.642(2)	0.45	12.49	12.17	3.5604

* Symmetry codes: (i) *x*, *y*, *z*; (ii) *x*, 1+*y*, *z*; (iii) -*x*+2, -*y*, -*z*+1; Cg (1) and Cg(2) represent the centroid of the rings (N1-C1-N2-C4-C5) and (C4-C5-C6-C7-C8-C9), respectively.

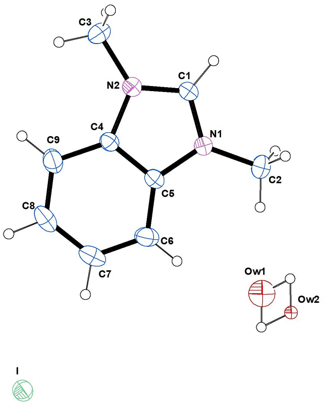

Figure 1. ORTEP view of 1,3-dimethyl-3*H*-benzimidazol-1-ium iodide monohydrate (DBZIW) with thermal ellipsoids at 50% probability level.

3. Results and discussion

3.1. Crystal structure

The compound under investigation, 1,3-dimethyl-3*H*-benzimidazol-1-ium iodide monohydrate (DBZIW), with the molecular formula $C_9H_{13}N_2IO$, crystallizes within a monoclinic system characterized by the space group $P2_1/c$ and a Z value of 4. The lattice parameters are defined as follows: a = 8.9323(4) Å, b = 7.1654(3) Å, c = 17.6425(8) Å, and β = 101.432(2) °. An ORTEP representation of the compound, complete with an atomic numbering scheme and thermal ellipsoids depicted at a 50% probability level, is presented in Figure 1. Table 3 provides detailed information regarding bond distances (Å), bond angles (°), and torsion angles (°) pertaining to non-hydrogen atoms. The stability of DBZIW is attributed to a network of interactions, including C-H···O, O-H···I, and π-π interactions. The geometrical parameters of both intramolecular and intermolecular hydrogen bond interactions are summarized in Table 4. In the context of molecular packing, the halogen iodine and the oxygen atoms of the water molecules play a pivotal role. These components alternate in contributing to the molecular packing by forming O-H···I dimers, wherein the oxygen of the water molecule acts as the donor, while iodine aligns to create a channel stabilized by O-H···I hydrogen bond interactions measuring 2.765(7) Å, as illustrated in Figure 2. Furthermore, intramolecular interactions involving the donor C2 via H2A and C6 via H6 with the acceptor oxygen of the water molecule (OW1) result in the formation of a pseudo ring characterized by $R^1_2(7)$ graph set motifs. Furthermore, a weak but significant π-π stacking interaction - is observed between the centroid of the five-membered imidazole ring (*x*, *y*, *z*) and the six-membered phenyl ring at coordinates (1-*x*, -1-*y*, 1-*z*), with a centroid-to-centroid distance of 3.642(2) Å, which further contributes to the molecular packing, as depicted in Figure 3.

3.2. Hirshfeld Surface analysis

The strength and function of hydrogen bonds and other intramolecular and intermolecular interactions have been calculated using Hirshfeld surface analysis, and their significance for the stability of the crystal lattice has been estimated. Figure 4a-c illustrate the Hirshfeld surface of the DBZIW molecule, showing that the surfaces have been mapped over a d_{norm} (range 0.03 to 0.95), d_i (range 1.06-2.59) and d_e (range 1.06-2.61). Red indicates shorter contacts, white indicates the contact surrounding the vdW (van deer Waals) separation, and blue indicates longer contacts on Hirshfeld

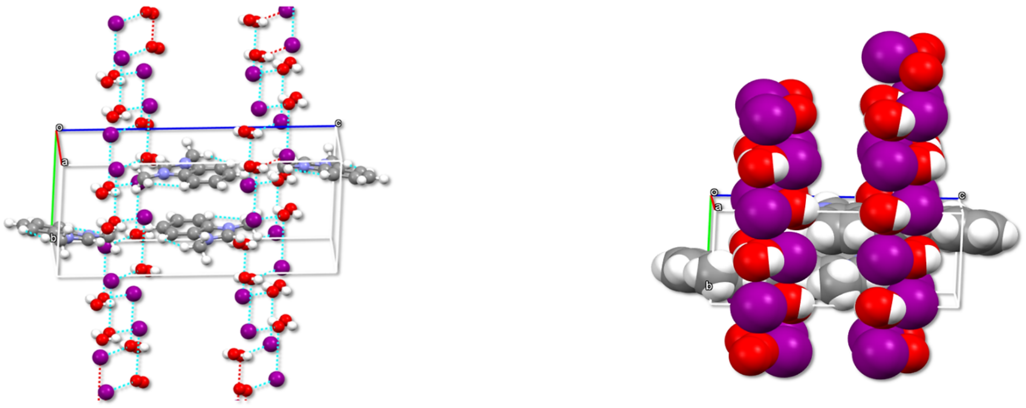
(a) (b)

Figure 2. The molecular packing by forming O-H···I dimer with water oxygen as the donor water molecule and iodine stacks in a fashion to form the channel hold by O-H···I hydrogen bond interactions shown (a) by ball- and stick-diagram and (b) by space-fill diagram.

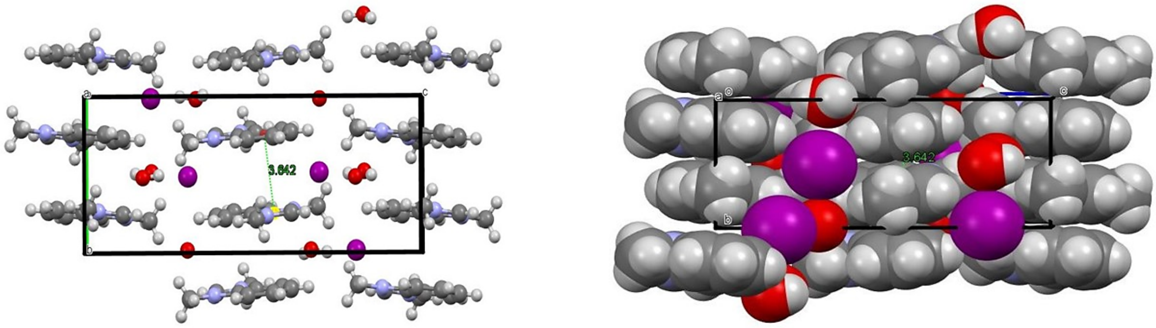

(a) (b)

Figure 3. The weak π–π stacked interaction involving the centroid of the five-membered imidazole ring with the six-membered phenyl ring with a Cg-Cg separation distance of 3.642(2) Å showing (a) the ball and stick diagram and (b) the space fill diagram.

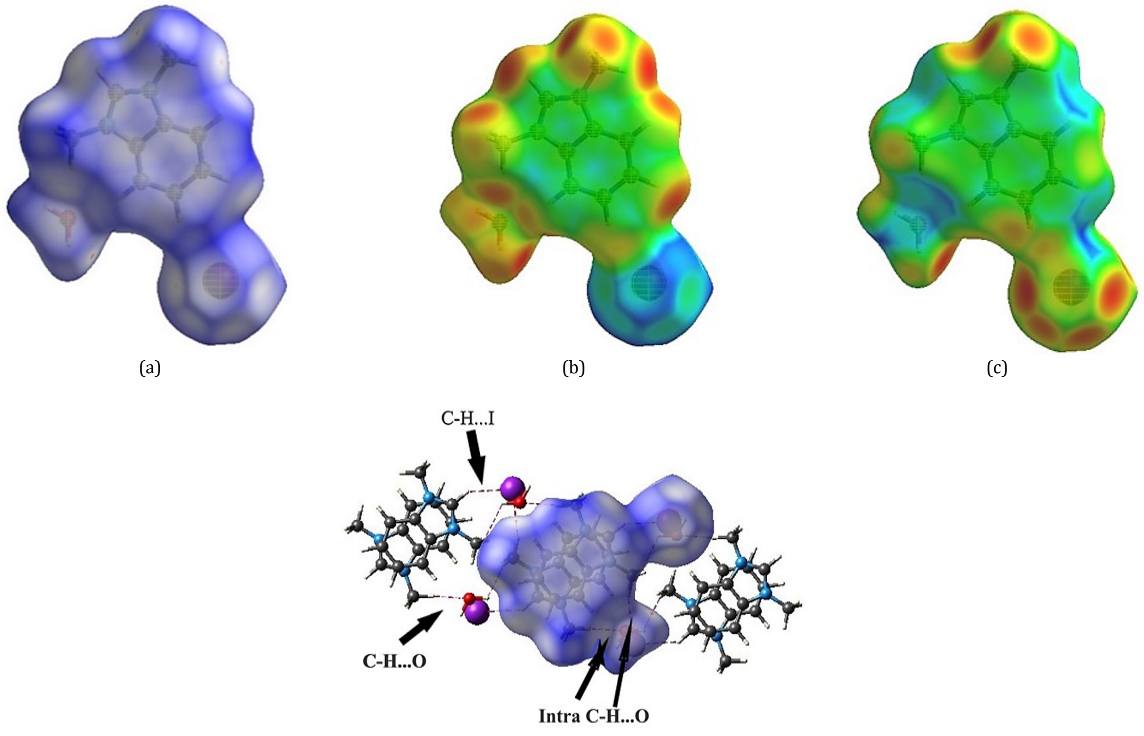
(a) (b) (c)

(d)

Figure 4. The Hirshfeld surface of the compound mapped with (a) d_{norm}, (b) d_{i}, and (c) d_{e} (d) d_{norm} surface depicts the close contacts of hydrogen bonds, indicating that intensive red spots correspond to intra- and intermolecular C-H···O and C-H···I hydrogen bonds.

Table 5. Molecular pairs and the interaction energies (kJ/mole) obtained from the energy framework calculation for the title molecule. The total energies, reported for the benchmarked energy model, are the sum of the four energy components. N is the number of equivalent neighbours; R is the distance between the molecular centroids (mean atomic position) in Å.

No	N	Symop	R	Electron density	E_{ele}	E_{pol}	E_{dis}	E_{rep}	E_{tot}
1	1	*-x, -y, -z*	8.94	B3LYP/6-31G(d, p)	-0.6	-0.4	-6.4	6.6	-2.5
2	0	*-x, -y, -z*	8.93	B3LYP/6-31G(d, p)	-0.4	-0.2	-2.6	0.6	-2.5
3	1	*x, y, z*	8.93	B3LYP/6-31G(d, p)	-0.5	-0.2	-5.3	1.6	-4.3
4	1	*-x, -y, -z*	3.81	B3LYP/6-31G(d, p)	3.1	-5.9	-46.5	20.7	-28.8
5	0	*-x, y+1/2, -z+1/2*	8.85	B3LYP/6-31G(d, p)	-0.4	-0.3	-4.3	2.7	-2.7
6	0	*-x, -y, -z*	3.79	B3LYP/6-31G(d, p)	3.1	-5.8	-46.0	20.2	-28.6
7	0	*-x, -y+1/2, z+1/2*	8.82	B3LYP/6-31G(d, p)	-0.6	-0.3	-6.3	2.3	-4.8

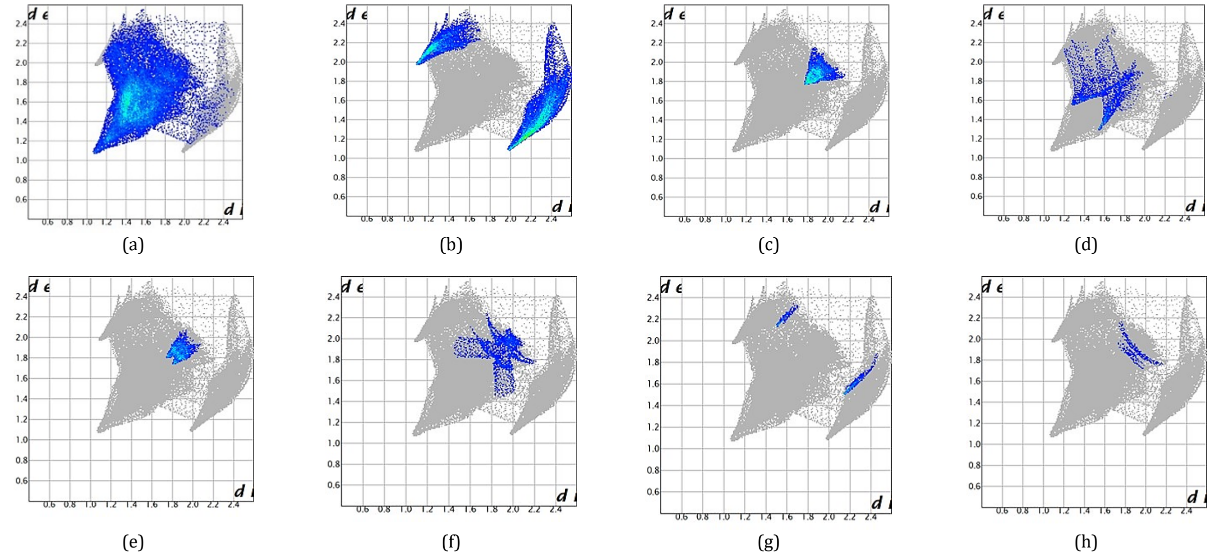

Figure 5. Atom-atom interactions and their contribution through two-dimensional fingerprint plots for the title compound, showing (a) H···H, (b) I···H/H···I, (c) C···C, (d) H···O/O···H, (e) N···C/C···N, (f) C···H/H···C, (g) I···O/O···I, and (h) H···N/N···H interactions.

surfaces 3D mapped with d_{norm}. The d_{norm} surface shows the close contacts between hydrogen bonds, indicating that intense red spots correspond to C-H···O and C-H···I hydrogen bond interactions, as revealed in Figure 4d.

The 2D fingerprint plots that estimate the different patterns of interaction in the crystalline network are illustrated in Figure 5. The intermolecular interactions H···H are most abundant in the crystalline frame [51.1% (Figure 5a)]. The H···I contact is the other most significant interaction due to the abundance of hydrogen on the molecular surface [27.5% (Figure 5b]. The van der Waals forces have a vital influence on the stabilization of the packaging in the crystalline structure. The Hirshfeld surfaces have been influenced by further intercontacts, including C···C (7.1%), O···H (4.6%), N···C (4.2%), C···H (3.8%), I···O (1.2%) and N···H (0.5%).

The stability of molecular structures is contingent upon the energy associated with intermolecular interactions, which were evaluated through energy framework analysis utilizing the Crystal Explorer21 software [35]. This analytical approach allows for the quantification of contacts within the crystal packing and their visualization as cylinders, with dimensions that correspond to the energy values of interactions between specific molecular pairs. The monomer wave function, derived from the B3LYP/6-31G(d,p) computational method via Crystal Explorer21, was employed to quantify these intermolecular interactions. The findings are presented alongside the probable intermolecular interactions occurring at various energy levels, as detailed in Table 5. We calculated the total interaction energy by taking into account the contributions from Coulombic, polarization, dispersion, and repulsion forces within a molecular cluster with a radius of 3.8 Å. As indicated in Table 5, the dispersion component emerged as the predominant contributor to each interaction, followed by the electrostatic, polarization, and repulsion energies, respectively. The energy frameworks provide a graphical representation of the magnitudes of intermolecular interaction energies, thereby facilitating visualization of the supramolecular architecture of the crystal structure. The interactions between molecular pairs are depicted as cylinders connecting the centroids of the respective molecules, the radius of each cylinder being proportional to the magnitude of the interaction energy. In Figure 6, the energy frameworks for electrostatic energy (E_{ele}) are illustrated as red cylinders (Figure 6a), dispersion energy (E_{dis}) as green cylinders (Figure 6b), and total energy (E_{tot}) in blue (Figure 6c), arranged to form zigzag ribbons extending along the *c*-axis. These cylinders reflect the relative strength of molecular packing in various orientations. The analysis clearly indicates that the dispersion energy, which is critical for molecular stability, constitutes the most significant contribution, a conclusion that aligns with observations made in analogous benzimidazole derivatives [41,42].

3.3. Computational studies

3.3.1. Optimized geometry

1,3-Dimethyl-3*H*-benzimidazol-1-ium (DBZ) (a), 1,3-dimethyl-3*H*-benzimidazol-1-ium monohydrate (DBZW) (b), structures were optimized at the B3LYP/6-311++G(d,p) level, and 1,3-dimethyl-3*H*-benzimidazol-1-ium iodine (DBZI) (c) and 1,3-dimethyl-3*H*-benzimidazol-1-ium iodide monohydrate (DBZIW) (d) structures were optimized at the B3LYP/Def2-TZVP method using Gaussian09 software, as shown in Figure 7. The diffuse function has been used for structure optimization by optimizing the benzimidazole derivatives with and without iodine and water; it was possible to reach a conclusion regarding the involvement of these molecules in the benzimidazole derivatives. Table 6 compares the calculated bond lengths and bond angles of (a) DBZ, (b) DBZW, (c) DBZI and (d) DBZIW with experimental X-ray diffraction data on bond lengths and bond angles.

Table 6. Bond lengths (Å) and bond angles (°) involving non-hydrogen atoms based on X-ray diffraction data (with estimated standard deviation in brackets) and computational calculations using Gaussian software.

Bond lengths (Å)	**Experimental, X-ray**	**Theoretical calculations using Gaussian software**			
	DBZIW	**DBZ** **B3LYP/6-311++G(d,p)**	**DBZW** **B3LYP/6-311++G(d,p)**	**DBZI** **B3LYP/Def2-TZVP**	**DBZIW** **B3LYP/Def2-TZVP**
N1- C1	1.330(4)	1.4685	1.4057	1.3459	1.3347
N1- C2	1.461(4)	1.4700	1.4475	1.4520	1.4579
N1- C5	1.392(4)	1.4122	1.3766	1.3904	1.3904
N2- C1	1.331(4)	1.4685	1.4098	1.3459	1.3383
N2- C3	1.463(4)	1.4700	1.4457	1.4520	1.4545
N2- C4	1.392(4)	1.4123	1.3820	1.3904	1.3910
C4- C5	1.378(5)	1.3904	1.4174	1.4025	1.4011
C4- C9	1.396(5)	1.3803	1.3899	1.3874	1.3888
C5- C6	1.386(5)	1.3804	1.3936	1.3874	1.3878
C6 -C7	1.364(6)	1.3978	1.4096	1.3899	1.3873
C7 -C8	1.412(7)	1.4058	1.3901	1.3983	1.4009
C8 -C9	1.371(6)	1.3979	1.4083	1.3899	1.3879
Bond Angles (°)	**X-ray**	**DBZ**	**DBZW**	**DBZI**	**DBZIW**
C1- N1- C5	108.1(3)	102.1075	109.8662	108.0200	108.1753
C1- N1- C2	125.8(3)	128.9462	124.1389	123.8108	125.3339
C5- N1- C2	126.1(3)	128.9462	125.0699	125.9717	126.1302
C1- N2- C4	108.0(3)	102.1093	109.5562	108.0198	108.0449
C1- N2- C3	126.3(3)	128.9454	123.0022	123.8107	124.5166
C4- N2- C3	125.7(3)	128.9454	124.6645	131.8677	126.1806
N1- C1- N2	110.2(3)	110.8848	104.9934	109.7621	110.4255
C5- C4- N2	106.9(3)	111.3471	107.1242	106.7050	106.5814
C5- C4- C9	121.9(3)	121.4253	121.0422	121.4273	121.4981
N2- C4- C9	131.1(3)	127.1956	131.8230	131.8677	131.9204
C4- C5- C6	122.2(3)	121.4188	121.0427	121.4274	121.6190
C4- C5- N1	106.7(3)	111.3538	107.2947	106.7049	106.5979
C6- C5- N1	131.2(3)	127.1952	131.6474	131.8678	131.7826
C7- C6- C5	116.3(4)	117.9550	117.6025	117.1083	116.8569
C6- C7- C8	121.9(4)	120.6229	121.2618	121.4639	121.5800
C9-C8- C7	121.7(4)	120.6153	121.2752	121.4639	121.5794
C8-C9- C4	115.9(4)	117.9551	117.7638	117.1083	116.8647
H11-OW1- H12	117(2)	-	105.2016	-	104.6342

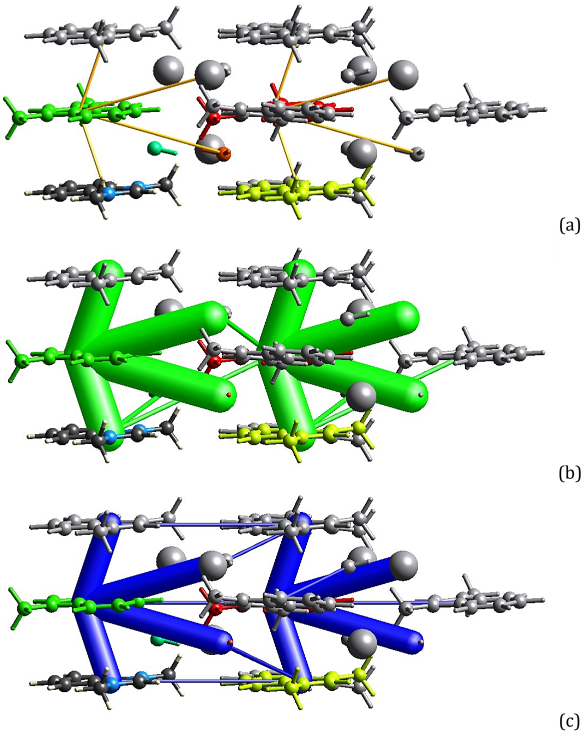

Figure 6. Energy-framework diagrams for (a) E_{elec}, (b) $E_{\text{disp.}}$ and (c) $E_{\text{tot.}}$ are shown as red, green and blue cylinders respectively. All diagrams use the same cylinder scale of 100 for energies. All energy frameworks as viewed along the *c* axes.

As shown in Table 6, the data show that all optimized bond lengths and bond angles were slightly larger than the values obtained by the experimental data from X-ray because the theoretical computational theoretical data related to the isolated molecule in the gas phase, while the experimental data were obtained in the solid phase. The highest difference in bond length is 0.132 Å (DBZ) for N1-C1, 0.0784 Å (DBZW) for N2- C1, 0.0253 Å (DBZI) and 0.0227 Å (DBZIW) for the C6-C7. The largest deviation of the bond angle occurred at the C1-N1-C5 angle (5.9925°) in DBZ, at the N1-C1-N2 angle (5.2066°) in DBZW, at the C4-N2-C3 angle (6.1167°) in DBZI, and at the C1-N2-C3 angle (1.7834°) in DBZIW.

Table 7. Correlation between the experimental and theoretical bond lengths and angles of (a) DBZ, (b) DBZW, (c) DBZI, and (d) DBZIW.

Parameters	DBZ B3LYP/6-311++G(d,p)	DBZW B3LYP/6-311++G(d,p)	DBZI B3LYP/Def2-TZVP	DBZIW B3LYP/Def2-TZVP
Bond lengths	0.9991	0.9994	0.9999	0.9999
Bond angles	0.9992	0.9993	0.9998	0.9994

Table 8. Mulliken charges (e) for the atoms of DBZ, DBZW, DBZI, and DBZWI molecules.

Atoms	DBZ	DBZW	DBZI	DBZIW
I	-	-	-0.6626	-0.8253
N1	-0.0535	0.0439	-0.0259	-0.0367
N2	-0.0536	0.0276	-0.0259	-0.0339
C1	-0.2661	-0.0556	-0.0155	0.0523
H1	0.1443	0.1528	0.2088	0.1929
C2	-0.3178	-0.3075	-0.2599	-0.3046
H21	0.1333	0.1884	0.1768	0.2046
H22	0.1569	0.1754	0.1285	0.1522
H23	0.1771	0.1395	0.1365	0.1436
C3	-0.3178	-0.3133	-0.2599	-0.2860
H31	0.1333	0.1465	0.1768	0.1588
H32	0.1772	0.1402	0.1364	0.1435
H33	0.1569	0.1833	0.1285	0.1625
C4	0.2568	0.0059	0.1333	0.1075
C5	0.2568	-0.1473	0.1333	0.0984
C6	-0.2372	-0.1123	-0.1916	-0.2143
H6	0.1341	0.1404	0.1245	0.1195
C7	-0.4333	-0.3990	-0.1076	-0.0985
H7	0.1508	0.1554	0.1202	0.1330
C8	-0.4334	-0.4842	-0.1077	-0.1292
H8	0.1508	0.1657	0.1202	0.2641
C9	-0.2372	-0.0719	-0.1916	-0.1716
H9	0.1629	0.1873	0.1245	0.2060
OW1	-	-0.5163	-	-0.6665
H11	-	0.2527	-	0.2947
H12	-	0.3026	-	0.3329

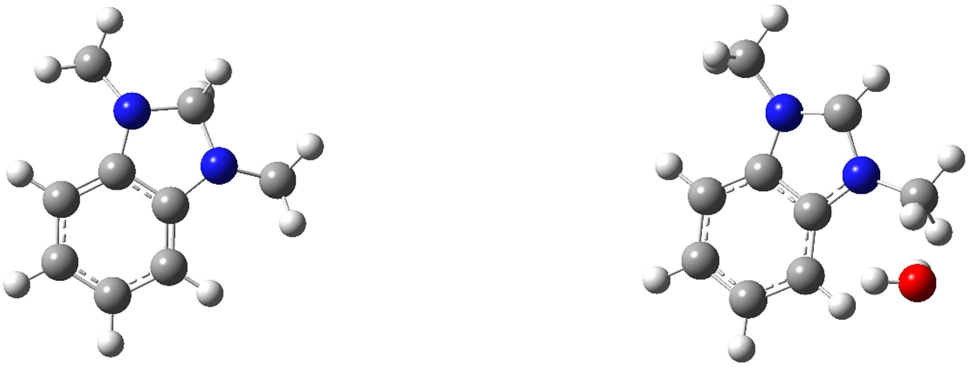

(a) DBZ (b) DBZW

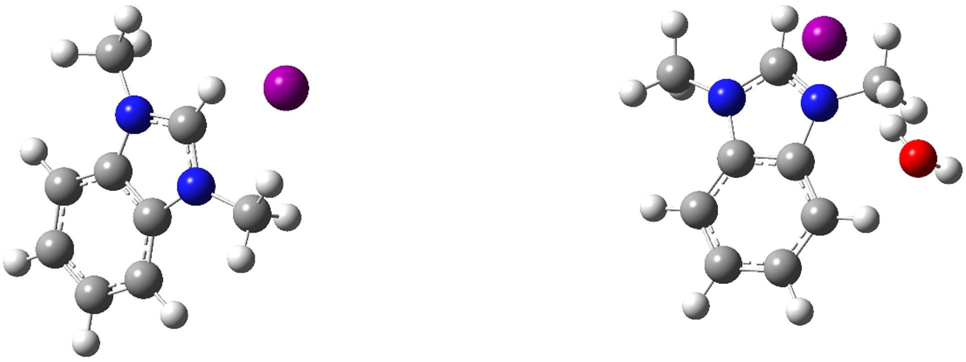

(c) DBZI (d) DBZIW

Figure 7. Optimized geometry structures (a) DBZ, (b) DBZW, (c) DBZI and (d) DBZIW.

For bond lengths, the root means square error (RMSE) of DBZ, DBZW, DBZI, and DBZWI is found to be approximately 0.0472, 0.0389, 0.0144, and 0.0117, respectively. For bond angles, DBZ, DBZW, DBZI and DBZWI have root mean square errors of 3.3425, 1.8371, 1.7600, and 0.6263°, respectively. This result shows that the theoretically calculated bond lengths and angles using the B3LYP/6-311++G(d,p) level and B3LYP/Def2-TZVP exhibit the strongest correlations with the experimental values (Table 7).

Table 9. HOMO and LUMO energies and global reactivity descriptors calculated for DBZ, DBZW, DBZI and DBZIW.

Parameters	DBZ	DBZW	DBZI	DBZWI
HOMO (eV)	-4.947	-4.714	-5.113	-5.090
LUMO (eV)	-0.409	-0.783	-1.728	-1.839
Energy gap (eV)	4.537	3.930	3.385	3.251
Ionization potential	4.947	4.714	5.113	5.090
Electron affinity	0.409	0.783	1.728	1.839
Chemical potential μ	-2.678	-2.749	-3.420	-3.465
Electron negativity χ	2.678	2.749	3.420	3.465
Hardness η (eV)	2.268	1.965	1.693	1.625
Softness (S)	0.220	0.254	0.295	0.308
Electrophilicity index (ω)	1.581	1.923	3.456	3.694
Total energy (eV)	-12511.5	-14574.8	-20601.1	-22682.2
Dipole moment (Debye)	2.316	2.331	9.156	9.342

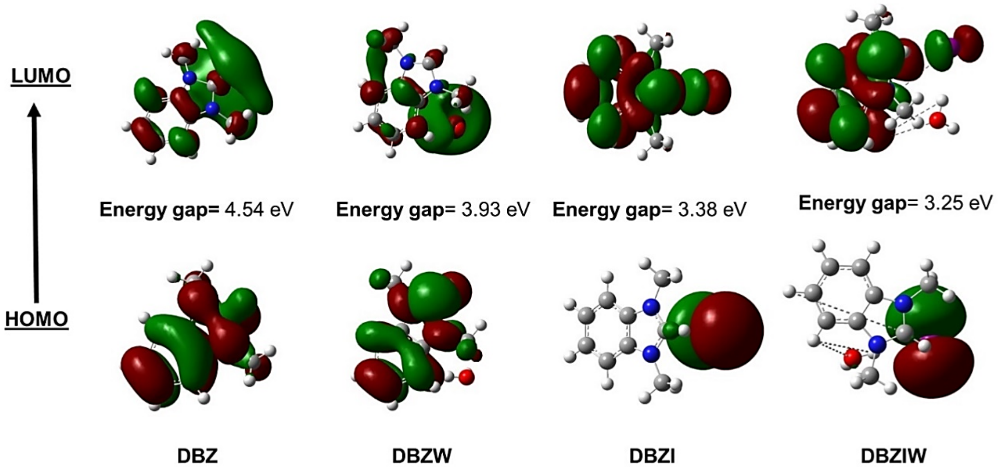

Figure 8. Highest occupied molecular orbital (HOMO) and lowest unoccupied molecular orbital (LUMO) of (a) DBZ, (b) DBZW, (c) DBZI and (d) DBZIW

3.3.2. Mulliken charge distributions

The Mulliken population analysis was used to determine the atomic charge values of the molecules (DBZ, DBZW, DBZI and DBZWI), which are summarised in Table 8. The charge on hydrogen atoms is positive. It should be noted that the DBZI and DBZWI molecules have an iodine atom and, compared to the other atoms in the molecule, have the highest negative charges of -0.6626 and -0.8253, respectively. The water molecules are backbone in the DBZW and DBZWI in the molecule and because of this has both DBZW (-0.5163) and DBZIW (-0.6665) oxygen atoms were negatively charged. In all of the benzimidazole derivatives, all nitrogen atoms had a negative charge, while all hydrogen atoms had a positive charge. Donor and acceptor atoms are signs that intra- and intermolecular hydrogen bonds are present in the solid-state phase.

3.3.3. FMO analysis

In order to understand the frontier effect of water and iodine, if present in benzimidazole derivatives, studies on the highest occupied molecular orbital (HOMO) and lowest unoccupied molecular orbital (LUMO) of the benzimidazole derivatives (a) DBZ, (b) DBZW, (c) DBZI, and (d) DBZIW were conducted. HOMO-LUMO explains a variety of reactions in conjugated systems and predicts the most reactive location in π-electron systems using the frontier electron density. FMO analysis is commonly used to describe the optical and electrical properties of organic compounds. To understand the nature of the electronic transition, the electron density plots of HOMO and LUMO are presented in Figure 8. The energy band gap values of the HOMO and LUMO of DBZ, DBZW, DBZI, and DBZIW are 4.537, 3.930, 3.385, and 3.251 eV, respectively. In molecular interactions, the HOMO represents electron donors, and its energy is related to the ionization potential (IP), while the LUMO represents electron acceptors, and its energy is related to the electron affinity (EA) [43,44]. The HOMO-LUMO energy gap, which is useful for determining molecular electrical transport properties, explains the charge transfer interaction within the molecule [45,46]. Table 9 lists the predicted HOMO and LUMO energies, as well as additional characteristics. Thus, it is clear from Table 9 that DBZ is hard, more stable, and less reactive, while compound DBZIW is soft, the least stable, and more reactive compared to the others. The HOMO-LUMO energy gap decreases from molecule DBZ to DBZI to DBZW, with the minimum energy gap achieved with the water and iodine substituents in DBZIW. Therefore, this substituent increases the reactivity of the benzimidazole derivative. From Figure 8, we observed that the electron density of the molecules' HOMO and LUMO frontier orbitals is primarily found on the fused benzimidazole moieties in DBZ and DBZW. This suggests that these locations act as electron-donating groups while forming coordination bonds with the unoccupied orbitals. Moreover, for the molecular structures of DBZI and DBZIW, the HOMO electron distribution is mainly located in the benzimidazole moiety, indicating that benzimidazole is responsible for electron donation, while the iodine and water molecules have a localized LUMO electron distribution. Consequently, these groups appear to be preferred locations for electron acceptance [47]. The HOMO-LUMO gap indicates the transition state of the molecules. In large conjugated π orbital systems, the mobility of the π electrons increases the energy distribution throughout the molecule, thus stabilizing it. Therefore, greater stability is correlated with smaller HOMO-LUMO gaps. Compared to the other structures discussed (DBZ, DBZI, and DBZW), the notable reduction of the gap in DBZIW indicates greater charge transfer and higher reactivity.

Table 10. The energy values of the DBZ, DBZW, DBZI, and DBZWI molecules obtained by the docking study.

Compound	7XW5	2XW7	4QT5
DBZ	-80.83	-165.83	-161.20
DBZW	-106.32	-205.06	-173.43
DBZI	-51.05	-188.38	-161.31
DBZWI	-111.13	-203.25	-191.91

Table 11. Measurement of the inhibition zone of the title compound *.

Organism	S_H	S_L	U_H	U_L
S. aureus	15	12	11	9
S. typhi	24	22	18	12

* S_H: Streptomycin high, U_H: Title compound (DBZIW) high, S_L: Streptomycin low, U_L: Title compound (DBZIW) low.

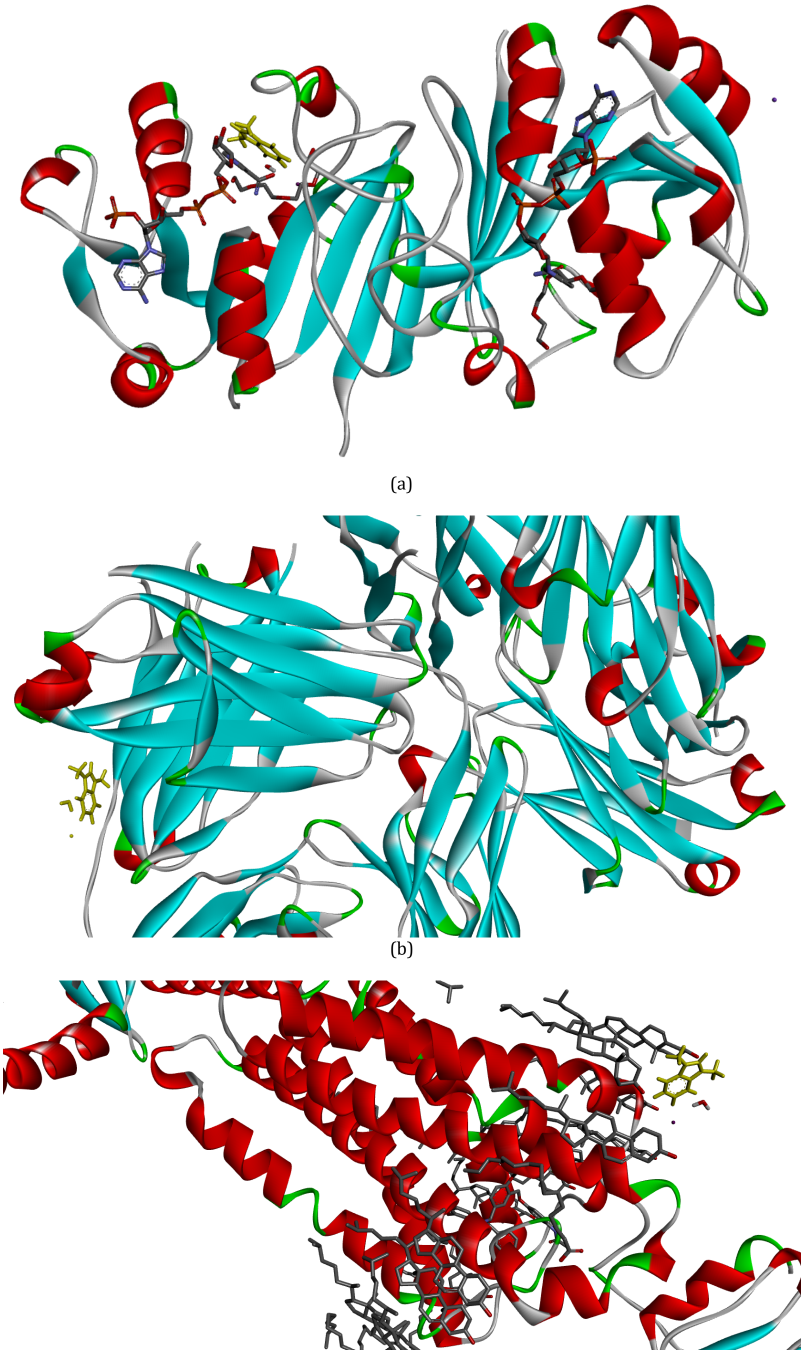

(a)

(b)

(c)

Figure 9. Molecular docking interactions between the molecule DBZWI with the thyroid stimulating hormone receptor (TSHR) (a) 2XW7, (b) 4QT5, and (c) 7XW7.

3.4. Molecular docking study

Thyroid function and disease are regulated by a protein called the thyroid stimulating hormone (TSH) receptor (TSHR). By stimulating the uptake of iodine into thyroid cells, which is necessary for the synthesis of thyroid hormones that depend on iodine to function correctly, TSHR plays a critical role in iodine metabolism. In other words, when TSH binds to TSHR, it sets off a series of events that increase iodine uptake and thyroid hormone production within the thyroid gland. The synthesized molecule DBZIW contains iodine. The function of thyroid stimulating hormones is where iodine has the most significant influence. Our objective is to determine the strength of the interaction between the ligand DBZIW's iodine and the protein receptor thyroid-stimulating hormone (TSHR). If the molecular interaction is strong, the ligand can be utilized as a drug to treat TSHR, which controls thyroid function and disease. We investigated a molecular docking study of 1,3-dimethyl-3*H*-benzimidazol-1-ium (DBZ), 1,3-dimethyl-3*H*-benzimidazol-1-ium monohydrate (DBZW), 1,3-dimethyl-3*H*-benzimidazol-1-ium iodine (DBZI), and 1,3-dimethyl-3*H*-benzimidazol-1-ium iodide monohydrate (DBZIW) to further explore the roles of water and iodine in the benzimidazole derivatives. We proposed other biological targets for our reported compounds, such as 2XW7, 4QT5, and 7XW7, which are pertinent to thyroid function and disease (TSHR). The Protein Bank (PDB) was used to download all protein receptors (PDB files). All aforementioned protein receptors underwent molecular docking experiments using the stated molecules (DBZ, DBZI, DBZW and DBZIW). The protein crystal structures for the thyroid stimulating hormone receptor (TSHR) were chosen (PDB IDs 2XW7, 4QT5, and 7XW7), and the Hex software [48] was employed to perform the docking of the benzimidazole derivatives. A docking calculation was performed to determine the docking score for the benzimidazole derivatives with the protein crystal structures separately using the HEX software. The energy values obtained from the docking study are tabulated in Table 10. When compared to other molecules (DBZ, DBZI, and DBZW), the molecule DBZIW showed compatibility with the receptors 2XW7, 4QT5, and 7XW7, achieving the best ligand scores of -203.25, -191.91, and -111.13 kJ/mol, respectively, as shown in Figure 9. As a result of the presence of water and iodine, DBZIW is more reactive compared to other molecular ligands. The docking score data, which also predict the activity of the pharmacological molecule, indicate the binding energy necessary to form a bond between the ligand and the receptor. The *in vitro* antibacterial activity of the synthesized DBZIW compound was evaluated using the dilution technique against bacterial strains and tabulated in Table 11.

4. Conclusion

In this work, we describe the crystal structure of 1,3-dimethyl-3*H*-benzimidazol-1-ium iodide monohydrate (DBZIW), which is capable of forming hydrogen bonds. DBZIW is organized in weak π–π stacked interactions involving the centroid of the five-membered imidazole ring with the six-membered phenyl ring, and is simultaneously stabilized by chains of intermolecular O-H⋯I dimer interactions with water molecules and iodine stacks, forming channels supported by O-H⋯I hydrogen bond interactions. Intermolecular hydrogen bonding interactions that contribute to molecular stability were highlighted by Hirshfeld surface analysis, and the 2D fingerprint map revealed the proportion of intermolecular contacts of the molecule, showing that H⋯H (51.1%) and I⋯H (27.5%) interactions are the most prevalent in the crystal lattice. The energy framework study revealed the corresponding energies for the intermolecular interactions involved; it was found that the dispersion energy contributes maximally for each molecular pair, ensuring the stability of the structure. To further investigate the molecular structure and the role of presence of the iodine ion and water in the molecular structure of DBZIW, we optimized the structures (DBZIW, DBZ, DBZI, and DBZW) using DFT methods. The iodine atom has the largest negative charge in the entire molecule, according to an analysis of Mulliken charge distributions, which may have led to the occurrence of interactions involving a particular atom of the molecule. The HOMO-LUMO orbital analysis and the energy band gap demonstrated charge transfer within the molecule, and the computed lowest HOMO-LUMO band gap for the molecule DBZIW indicates intriguing electronic properties. The thyroid-stimulating hormone receptor (TSHR) (PDB IDs 2XW7, 4QT5, and 7XW7) was selected for molecular docking analysis, revealing a better docking score for the benzimidazole derivative (DBZWI) with the 4QT5 protein crystal, suggesting more advantages for further pharmacological applications, especially for the iodine molecule.

Acknowledgements

We thank the Department of Science and Technology (DST), New Delhi for supporting the Fund for Improvement of S&T Infrastructure in Universities and Higher Educational Institutions (FIST) project at the Department of Physics, Sardar Patel University, Vallabh Vidyanagar, Gujarat, India, by providing the single-crystal X-ray diffractometer (Kappa Apex -II) equipment.

Supporting information S

CCDC-1508765 contains the supplementary crystallographic data for the compound. These data can be obtained free of charge via http://www.ccdc.cam.ac.uk/conts/retrieving.html , or from the Cambridge Crystallographic Data Centre, 12 Union Road, Cambridge CB2 1EZ,UK;fax: (+44) 1223-336-033; or e-mail: deposit@ccdc.cam.ac.uk.

Disclosure statement DS

Conflict of interest: The authors declare that they have no conflict of interest.
Ethical approval: All ethical guidelines have been adhered.
Sample availability: Samples of the compounds are available from the author.

CRediT authorship contribution statement CR

Conceptualization: Urmila Patel, Sahajkumar Anilkumar Gandhi; Saurabh Soni; Methodology: Sahajkumar Anilkumar Gandhi, Deepali Kotadia; Software: Urmila Patel, Sahajkumar Anilkumar Gandhi; Validation: Sahajkumar Anilkumar Gandhi, Deepali Kotadia; Formal Analysis: Sahajkumar Anilkumar Gandhi, Deepali Kotadia, Saurabh Soni; Investigation: Sahajkumar Anilkumar Gandhi, Deepali Kotadia, Saurabh Soni; Resources: Sahajkumar Anilkumar Gandhi, Deepali Kotadia; Data Curation: Sahajkumar Anilkumar Gandhi, Deepali Kotadia; Writing - Original Draft: Sahajkumar Anilkumar Gandhi; Writing - Review and Editing: Sahajkumar Anilkumar Gandhi, Urmila Patel; Visualization: Sahajkumar Anilkumar Gandhi; Funding acquisition: Urmila Patel, Saurabh Soni; Supervision: Urmila Patel, Sahajkumar Anilkumar Gandhi; Project Administration: Urmila Patel.

ORCID and Email

Sahajkumar Anilkumar Gandhi
sahajg7@gmail.com
https://orcid.org/0000-0002-3650-3780
Saurabh Soni
soni_b21@yahoo.co.in
https://orcid.org/0000-0002-7584-4916
Urmila Patel
u_h_patel@yahoo.com
https://orcid.org/0000-0003-4883-1391
Deepali Kotadia
deepalikotadia@gmail.com
https://orcid.org/0009-0000-3738-7745

References

[1]. Ayhan-Kilcigil, G.; Kus, C.; Çoban, T.; Can-Eke, B.; Iscan, M. Synthesis and Antioxidant Properties of Novel Benzimidazole Derivatives. *J. Enzyme Inhib. Med. Chem.* **2004**, *19* (2), 129–135.

[2]. Kuş, C.; Sözüdönmez, F.; Can-Eke, B.; Çoban, T. Antioxidant and Antifungal Properties of Benzimidazole Derivatives. *Z. fÃ¼r Naturforsch. C* **2010**, *65* (9-10), 537–542.

[3]. Rao, H. S.; Vasantham, K. Nitroketene dithioacetal chemistry: Synthesis of coumarins incorporating nitrothiophene moiety. *J. Chem Sci* **2011**, *123* (4), 411–420.

[4]. Ates-Alagoz, Z. Antioxidant Activities of Retinoidal Benzimidazole Or Indole Derivatives in In Vitro Model Systems. *CMC.* **2013**, *20* (36), 4633–4639.

[5]. Ayhan-Kilcigil, G.; Kuş, C.; Çoban, T.; Özdamar, E. D.; Can-Eke, B. Identification of a Novel Series of *N*-Phenyl-5-[(2-phenyl benzimidazol-1-yl)methyl]-1,3,4-oxadiazol-2-amines as Potent Antioxidants and Radical Scavengers. *Arch. Pharm.* **2014**, *347* (4), 276–282.

[6]. Cao, Q.; Xie, Z.; Dong, Q.; Ma, Q.; Yue, T.; Wang, L.; Wang, D. Studied on highly sensitive fluorescent sensors for Fe3+, Nitrobenzene and dye adsorption properties of Ln-MOFs based on benzimidazole carboxylic acid ligand. *J. Mol. Struct.* **2023**, *1293*, 136246.

[7]. Sharma, V.; Banerjee, B.; Sharma, A.; Gupta, V. K. Synthesis, X-ray crystal structure, Hirshfeld surface analysis, and molecular docking studies of DMSO/H2O solvate of 5-chlorospiro[indoline-3,7'-pyrano[3,2-c:5,6-c']dichromene]-2,6',8'-trione. *Eur. J. Chem.* **2021**, *12* (4), 382–388.

[8]. Adardour, M.; Ait Lahcen, M.; Oubahmane, M.; Ettahiri, W.; Hdoufane, I.; Bouamama, H.; Alanazi, M. M.; Cherqaoui, D.; Taleb, M.; Garcia, E. Z.; Baouid, A. Design, Synthesis, Molecular Modeling and Biological Evaluation of Novel Pyrazole Benzimidazolone Derivatives as Potent Antioxidants. *Pharmaceuticals* **2023**, *16* (12), 1648.

[9]. Ettahiri, W.; Salim, R.; Adardour, M.; Ech-chihbi, E.; Yunusa, I.; Alanazi, M. M.; Lahmidi, S.; Barnossi, A. E.; Merzouki, O.; Iraqi Housseini, A.; Rais, Z.; Baouid, A.; Taleb, M. Synthesis, Characterization, Antibacterial, Antifungal and Anticorrosion Activities of 1,2,4-Triazolo[1,5-a]quinazolinone. *Molecules* **2023**, *28* (14), 5340.

[10]. Ettahiri, W.; Adardour, M.; Alaoui, S.; Allah, A. E.; Aichouch, M.; Salim, R.; Ramli, Y.; Bouyahya, A.; Taleb, M. Recent advance in the development of N-heterocyclic derivatives as anti-SARS-CoV-2 inhibitors: A review. *Phytochem. Lett.* **2024**, *61*, 247–269.

[11]. Horiuchi, S.; Kagawa, F.; Hatahara, K.; Kobayashi, K.; Kumai, R.; Murakami, Y.; Tokura, Y. Above-room-temperature ferroelectricity and antiferroelectricity in benzimidazoles. *Nat Commun* **2012**, *3* (1), 1308 https://doi.org/10.1038/ncomms2322.

[12]. Cosby, T.; Holt, A.; Griffin, P. J.; Wang, Y.; Sangoro, J. Proton Transport in Imidazoles: Unraveling the Role of Supramolecular Structure. *J. Phys. Chem. Lett.* **2015**, *6* (19), 3961–3965.

[13]. Nagamani, C.; Versek, C.; Thorn, M.; Tuominen, M. T.; Thayumanavan, S. Proton conduction in 1*H*-1,2,3-triazole polymers: Imidazole-like or pyrazole-like? *J. Polym. Sci. A. Polym. Chem.* **2010**, *48* (9), 1851–1858.

[14]. Kerru, N.; Gummidi, L.; Maddila, S.; Gangu, K. K.; Jonnalagadda, S. B. A Review on Recent Advances in Nitrogen-Containing Molecules and Their Biological Applications. *Molecules* **2020**, *25* (8), 1909.

[15]. Ettahiri, W.; Adardour, M.; Ech-chihbi, E.; Azam, M.; Salim, R.; Dalbouha, S.; Min, K.; Rais, Z.; Baouid, A.; Taleb, M. 1,2,3-triazolyl-linked benzimidazolone derivatives as new eco-friendly corrosion inhibitors for mild steel in 1 M HCl solution: Experimental and computational studies. *Colloids Surf. A: Physicochem. Eng. Asp.* **2024**, *681*, 132727.

[16]. Ech-chihbi, E.; Adardour, M.; Ettahiri, W.; Salim, R.; Ouakki, M.; Galai, M.; Baouid, A.; Taleb, M. Surface interactions and improved corrosion resistance of mild steel by addition of new triazolyl-benzimidazolone derivatives in acidic environment. *J. Mol. Liq.* **2023**, *387*, 122652.

[17]. Salim, R.; Ech-chihbi, E.; Ettahiri, W.; Hammouti, B.; Rais, Z.; Taleb, M. Industrial Corrosion Inhibitors: Food Waste as Ideal Substitutes. *Mater. Horiz.: Nat. Nanomater.* **2024**, 231–266.

[18]. Ettahiri, W.; Adardour, M.; Ech-chihbi, E.; Dalbouha, S.; Hammouti, B.; Rais, Z.; Baouid, A.; Taleb, M. Regio- and chemoselective synthesis of new isoxazolyl-linked benzimidazolones via 1,3-dipolar cycloaddition: Characterization, corrosion studies, density functional theory, and Monte Carlo simulations. *Fuel* **2024**, *371*, 132058.

[19]. Salim, R.; Adardour, M.; Ettahiri, W.; Ech-chihbi, E.; Hammouti, B.; Azam, M.; Min, K.; Baouid, A.; Taleb, M. Computational and electrochemistry of effective triazolyl-benzimidazolone inhibitors in aggressive environment. *Sustain. Mater. Technol.* **2024**, *39*, e00862.

[20]. Aydogdu, I. S.; Gumus, I.; Arslan, H. Hirshfeld surface and theoretical studies of 2,2,2-trichloro-N,N-bis(2-(2,2,2-trichloroacetamido) phenyl)acetamide compound. *Eur. J. Chem.* **2019**, *10* (4), 323–335.

[21]. Tanaka, A.; Nakashima, K.; Miura, Y. DFT studies of N-alkoxyaminyl radicals: ESR parameters, UV–vis absorptions and generations. *Tetrahedron* **2011**, *67* (12), 2260–2268.

[22]. Patel, U. H.; Gandhi, S. A.; Barot, V. M.; Patel, M. C. 3-(2-Chloro-3-hydroxy-4-methoxyphenyl)-1-(4,5-dimethoxy-2-methylphenyl)prop-2-en-1-one. *Acta Crystallogr E. Struct Rep Online* **2012**, *68* (10), o2926–o2927.

[23]. Malek, T. J.; Gandhi, S. A.; Barot, V.; Patel, M.; Patel, U. H. Crystal structure and Hirshfeld surface analysis of methyl 4-[(*E*)-2-(5-bromo-2-methoxybenzylidene)hydrazinyl]-3-nitrobenzoate. *Acta Crystallogr E. Cryst Commun* **2018**, *74* (9), 1239–1243.

[24]. Patel, U. H.; Gandhi, S. A.; Barot, V. M.; Patel, M. C. Synthesis, Spectroscopic Investigations, Quantum Chemical Studies (Ab-initio & DFT) and Antimicrobial Activities of 3-(3-Chloro-4,5-dimethoxy-phenyl)-1-(4, 5-dimethoxy-2-methyl-Phenyl) prop-2-en-1-one. *CSTA.* **2013**, *02* (04), 167–175.

[25]. Patel, U. H.; Gandhi, S. A.; Barot, V. M.; Patel, M. C. A comparative study of novel chalcone derivative by X-ray and quantum chemical calculations (Ab-initio and DFT): Experimental and theoretical approach. *Mol. Cryst. Liq. Cryst.* **2016**, *624* (1), 190–204.

[26]. Gandhi, S. A.; Patel, U. H.; Modh, R. D.; Naliyapara, Y.; Patel, A. S. Quantum Chemical Calculations (Ab Initio & DFT), Hirshfeld Surface Analysis, Crystal Structure and Molecular Docking Study of 2-Chloro-4-(4-fluoro-phenyl)-6-isopropyl-pyrimidine-5-carboxylic Acid Methyl Ester. *J. Chem Crystallogr* **2016**, *46* (10-12), 387–398.

[27]. Bruker (2002). SAINT. Bruker AXS Inc., Madison, Wisconsin, USA.

[28]. Sheldrick, G. M. Crystal structure refinement with *SHELXL*. *Acta Crystallogr C. Struct Chem* **2015**, *71* (1), 3–8.

[29]. Sheldrick, G. M. A short history of *SHELX*. *Acta Crystallogr A. Found Crystallogr* **2007**, *64* (1), 112–122.

[30]. Ditchfield, R.; Hehre, W. J.; Pople, J. A. Self-Consistent Molecular-Orbital Methods. IX. An Extended Gaussian-Type Basis for Molecular-Orbital Studies of Organic Molecules. *J. Chem. Phys.* **1971**, *54* (2), 724–728.

[31]. Lee, C.; Yang, W.; Parr, R. G. Development of the Colle-Salvetti correlation-energy formula into a functional of the electron density. *Phys. Rev. B.* **1988**, *37* (2), 785–789.

[32]. Zhu, Y.; Alqahtani, S.; Hu, X. An Assessment of Dispersion-Corrected DFT Methods for Modeling Nonbonded Interactions in Protein Kinase Inhibitor Complexes. *Molecules* **2024**, *29* (2), 304.

[33]. Frisch, M. J.; Trucks, G. W.; Schlegel, H. B.; Scuseria, G. E.; Robb, M. A.; Cheeseman, J. R.; Montgomery, J. A.; Vreven, T.; Kudin, K. N.; Burant, J. C.; Millam, J. M.; Iyengar, S. S.; Tomasi, J.; Barone, V.; Mennucci, B.; Cossi, M.; Scalmani, G.; Rega, N.; Petersson, G. A.; Nakatsuji, H.; Hada, M.; Ehara, M.; Toyota, K.; Fukuda, R.; Hasegawa, J.; Ishida, M.; Nakajima, T.; Honda, Y.; Kitao, O.; Nakai, H.; Klene, M.; Li, X.; Knox, J. E.; Hratchian, H. P.; Cross, J. B.; Adamo, C.; Jaramillo, J.; Gomperts, R.; Stratmann, R. E.; Yazyev, O.; Austin, A. J.; Cammi, R.; Pomelli, C.; Ochterski, J. W.; Ayala, P. Y.; Morokuma, K.; Voth, G. A.; Salvador, P.; Dannenberg, J. J.; Zakrzewski, V. G.; Dapprich, S.; Daniels, A. D.; Strain, M. C.; Farkas, O.; Malick, D. K.; Rabuck, A. D.; Raghavachari, K; Foresman, J. B.; Ortiz, J. V.; Cui, Q.; Baboul, A. G.; Clifford, S.; Cioslowski, J.; Stefanov, B. B.; Liu, G.; Liashenko, A.; Piskorz, P.; Komaromi, I.; Martin, R. L.; Fox, D. J.; Keith, T.; Al-Laham, M. A.; Peng, C. Y.; Nanayakkara, A.; Challacombe, M.; Gill, P. M. W.; Johnson, B.; Chen, W.; Wong, M. W.; Gonzalez, C.; Pople, J. A. Gaussian 09, Revision A.02; Gaussian, Inc., Wallingford CT, 2004.

[34]. Dennington, R.; Keith, T. A.; Millam, J. M. GaussView, Version 6, Semichem Inc.; Shawnee Mission, KS, 2016.

[35]. Spackman, P. R.; Turner, M. J.; McKinnon, J. J.; Wolff, S. K.; Grimwood, D. J.; Jayatilaka, D.; Spackman, M. A. *CrystalExplorer*: a program for Hirshfeld surface analysis, visualization and quantitative analysis of molecular crystals. *J. Appl Crystallogr* **2021**, *54* (3), 1006–1011.

[36]. Mohabbat, A.; Salama, J.; Seiffert, P.; Boldog, I.; Janiak, C. Single-Crystal Structure Analysis of Dicarboxamides: Impact of Heteroatoms on Hydrogen Bonding of Carboxamide Groups. *Crystals* **2024**, *14* (9), 811.

[37]. Chen, C.; Hubbard, P. A.; Salazar, L. M.; McLachlan, S. M.; Murali, R.; Rapoport, B. Crystal Structure of a TSH Receptor Monoclonal Antibody: Insight Into Graves' Disease Pathogenesis. *Mol. Endocrinol.* **2015**, *29* (1), 99–107.

[38]. Berman, H.; Henrick, K.; Nakamura, H. Announcing the worldwide Protein Data Bank. *Nat Struct Mol Biol* **2003**, *10* (12), 980–980.

[39]. Meng, X.; Zhang, H.; Mezei, M.; Cui, M. Molecular Docking: A Powerful Approach for Structure-Based Drug Discovery. *CAD.* **2011**, *7* (2), 146–157.

[40]. Ghoorah, A. W.; Devignes, M.; Smaïl-Tabbone, M.; Ritchie, D. W. Protein docking using case-based reasoning. *Proteins* **2013**, *81* (12), 2150–2158.

[41]. Azgaou, K.; Ettahiri, W.; Ech-chihbi, E.; Adardour, M.; Azam, M.; Benmessaoud, M.; Baouid, A.; Min, K.; El Hajjaji, S. Experimental and computational study of newly synthesized benzimidazole derivatives as corrosion inhibitors for mild steel in 1.0 M HCl: Electrochemical, surface studies, DFT modeling, and MC simulation. *J. Electroanal. Chem.* **2024**, *974*, 118699.

[42]. Guendouz, A.; Ettahiri, W.; Adardour, M.; Lazrak, J.; Assiri, E. H.; Taleb, A.; Hammouti, B.; Rais, Z.; Baouid, A.; Taleb, M. New Benzimidazole derivatives as efficient organic inhibitors of mild steel corrosion in

hydrochloric acid medium: Electrochemical, SEM/EDX, MC, and DFT studies. *J. Mol. Struct.* **2025**, *1321*, 139901.

[43]. Miar, M.; Shiroudi, A.; Pourshamsian, K.; Oliaey, A. R.; Hatamjafari, F. Theoretical investigations on the HOMO–LUMO gap and global reactivity descriptor studies, natural bond orbital, and nucleus-independent chemical shifts analyses of 3-phenylbenzo[*d*]thiazole-2(3*H*)-imine and its *para*-substituted derivatives: Solvent and substituent effects. *J. Chem. Res.* **2020**, *45* (1-2), 147–158.

[44]. Parr, R. G.; Szentpály, L. v.; Liu, S. Electrophilicity Index. *J. Am. Chem. Soc.* **1999**, *121* (9), 1922–1924.

[45]. Parr, R. G.; Pearson, R. G. Absolute hardness: companion parameter to absolute electronegativity. *J. Am. Chem. Soc.* **1983**, *105* (26), 7512–7516.

[46]. Padmaja, L.; Ravikumar, C.; Sajan, D.; Hubert Joe, I.; Jayakumar, V. S.; Pettit, G. R.; Faurskov Nielsen, O. Density functional study on the structural conformations and intramolecular charge transfer from the vibrational spectra of the anticancer drug combretastatin-A2. *J. Raman Spectroscopy* **2008**, *40* (4), 419–428.

[47]. Ettahiri, W.; El Moutaouakil Ala Allah, A.; Lazrak, J.; Safir, E.; Yadav, K.; Hammouti, B.; Obaidullah, A.; Rais, Z.; Ramli, Y.; Taleb, M. Synthesis, characterization, theoretical, and experimental evaluation of novel imidazolone – based compounds as eco-friendly corrosion inhibitors for mild steel. *J. Ind. Eng. Chem.* **2024**, *140*, 631–646.

[48]. Ritchie, D. W. Hex 6.3 User Manual: Protein Docking Using Spherical Polar Fourier Correlations, 1996-2010.